J. Fluid Mech. (1982), *vol.* 122, *pp.* 315–338
Printed in Great Britain

Large-amplitude free and driven drop-shape oscillations: experimental observations

By E. TRINH AND T. G. WANG
Jet Propulsion Laboratory, California Institute of Technology, Pasadena, CA 91109

(Received 6 May 1981 and in revised form 26 October 1981)

A quantitative study of some nonlinear aspects of drop-shape oscillations in a liquid–liquid system has been completed. The results suggest a soft nonlinearity in the fundamental resonant mode frequency as the oscillation amplitude is increased. Indications of an increase in the rate of decay have also been obtained. A study of the internal flow fields has revealed patterns of circulation not present at low amplitude.

1. Introduction

The dynamics of small-amplitude drop-shape oscillations of liquid drops have been extensively studied in both theory and practice (Miller & Scriven 1968; Marston 1980; Trinh, Zwern & Wang 1982). Linear theories dealing with the problem of drop oscillations in immiscible liquid hosts have been shown to yield predictions that are in general agreement with experimental results. Empirically observed departures from the theoretical predictions have often been attributed to effects associated with large-amplitude oscillations. Possible observations of such phenomena have been reported, but no rigorous analysis has been possible because all the relevant parameters had not been under the experimenter's control. This paper deals with the quantitative and qualitative investigations of such nonlinear characteristics. Accurate determinations of the resonance frequency, the oscillation amplitude, the decay constant, the static equilibrium shapes, and the detailed motion during steady-state oscillations and free decay have been made possible by an acoustic-levitation technique using radiation-pressure modulation (Marston & Apfel 1979).

After a discussion of the experimental method and of the various effects of the acoustic field during driven oscillations, we shall treat the amplitude dependence of both the resonance frequency and the decay constant. The variation of the resonance frequency with the static equilibrium shape will also be discussed together with the asymmetries in the time distribution of the two configurations of the drop undergoing acoustically driven oscillations in the fundamental mode. The swept frequency response of a driven drop also appears to yield some interesting characteristics. Finally, the internal flow field of a vibrating drop has been shown to possess additional properties not found in the small-amplitude region.

The rigorous interpretation of the observed phenomena is not possible at the present time owing to the lack of a nonlinear theory. The detailed analysis of the phenomena makes it necessary to isolate the interfering effects of the acoustic field, even though these factors only exert a small perturbation upon the motion of the liquid drop.

The scope of this work is restricted to the consideration of one of the lowest modes of oscillation: the axisymmetric oblate–prolate vibration.

2. Summary of the results obtained for small-amplitude oscillations

In a previous paper we have reported the results of experimental measurements of the resonance frequency for the first few modes, as well as of the damping constant for the fundamental mode under the restriction of small-amplitude oscillations (Trinh *et al.* 1982). Both the drop diameter and the viscosity of the inner and outer liquids were varied.

A reasonable agreement with the theoretical predictions concerning the relationship of the frequencies of the first four resonant modes was obtained for low-viscosity liquids (kinematic viscosity less than 5 cSt). The radius dependence of the fundamental mode was also determined experimentally for drop viscosities from 1·2 to 120 cSt and radii between 0·2 and 0·4 cm. The results have revealed that the power law $f_2 \propto R^{-1.5}$ was a good approximation (within 5 %) for all the cases investigated.

The experimental results for the damping constant were also in general agreement with the theoretical treatments for the viscosity range investigated. Finally, a qualitative study of the internal flow fields of drops oscillating at small amplitude has revealed a quasi-potential flow with no apparent circulation.

3. The experimental technique

3.1. *Acoustic-field configurations and drop positions*

We have used acoustic radiation-pressure forces to trap a drop at a stable position, to deform its equilibrium shape, and to drive it into oscillation. A detailed description of the apparatus and method has been given elsewhere (Trinh *et al.* 1980).

Figure 1 (*a*) describes idealized experimental conditions involving a drop of approximately 1 cm in diameter levitated by an acoustic standing wave established in a liquid-filled rectangular cavity (9 × 9 × 13 cm). A standing wave at 22 kHz used in this work has a half-wavelength equal to about 3·4 cm in water at about 22 °C. The vertical axis shown in figure 1 (*a*) is taken as the symmetry axis, and the drop position shown is that relevant to the case of a liquid having higher compressibility and density than the host liquid. For such a liquid combination and wave field the acoustic radiation forces will drive the drop towards a position of maximum acoustic pressure. The magnitude of this force increases with vertical distance from the local pressure antinode. One might also note that there exist two components to the force: the main part consists of a vertically directed component, and the other part, much smaller in magnitude, exerts a centring action tending to drive the drop towards the central symmetry axis. The effects of such a small centring force will be neglected in the following discussion.

Figure 1 (*b*) shows the same idealized situation, except for the addition of a 66 kHz standing wave. The descriptions provided by both figures 1 (*a*, *b*) are idealized because they do not take into account the effects of the levitated drop on the sound fields. With drops of such size one would expect a modification of the acoustic-pressure distribution.

3.2. *Equilibrium drop shapes and oscillation drives*

In the case of a 22 kHz wave (figure 1 *a*), it is not difficult to realize that a spherical drop can be distorted into an oblate spheroid as the acoustic pressure is increased. The liquid within the drop is drawn closer to the pressure antinode, thereby flattening the

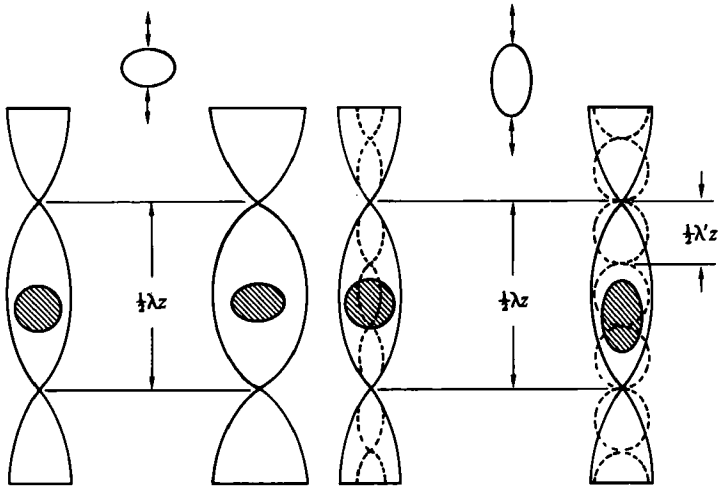

FIGURE 1. Schematic representation of an approximately 1 cm³ drop trapped in a 22 kHz standing acoustic wave (*a*). As the acoustic pressure is increased the radiation pressure forces drive the drop into an oblate spheroidal shape. In (*b*) the drop is placed in two superposed standing waves (22+66 kHz). As the amplitude of the higher frequency wave is increased the drop is shown to be deformed into a prolate shape. The distortion of the acoustic fields is neglected.

drop at the poles. A time modulation of the pressure intensity will provide a periodic squeezing action to drive steady-state shape oscillations. A theoretical treatment of the action of the acoustic radiation-pressure force on a levitated liquid sphere has been provided recently (Marston, Loporto-Arione & Pullen 1981), and predicts a distortion of the same nature.

When a 66 kHz standing wave is introduced, an initially spherical drop may take two different shapes, depending upon its acoustic properties and size. The sphere may deform into an oblate spheroid, as in the preceding case, or it may be elongated into a prolate spheroid because of the action of two neighbouring pressure antinodes. Modulation of the pressure will then provide an additional driving mechanism opposite to that described previously: the drop will be periodically elongated.

3.3. *Effects of the acoustic fields on the drop motion*

3.3.1. *Single standing wave.* In the work described in this paper, the modulation of the acoustic force is obtained electronically through a balanced modulator. In the simplest case, a 22 kHz sinusoidal signal (frequency f_c) is multiplied by a second sine wave of much lower frequency (f_m).

The voltage across the transducer terminals is then

$$V_T = V_c \sin(2\pi f_c t)\cos(2\pi f_m t). \tag{1}$$

The acoustic pressure is proportional to this voltage for linear operation of the transducer. The radiation pressure force is proportional to the time average of the acoustic pressure squared, and can be described as

$$P_r \sim \langle P^2_{\text{acoustic}} \rangle \sim \cos^2(2\pi f_m t). \tag{2}$$

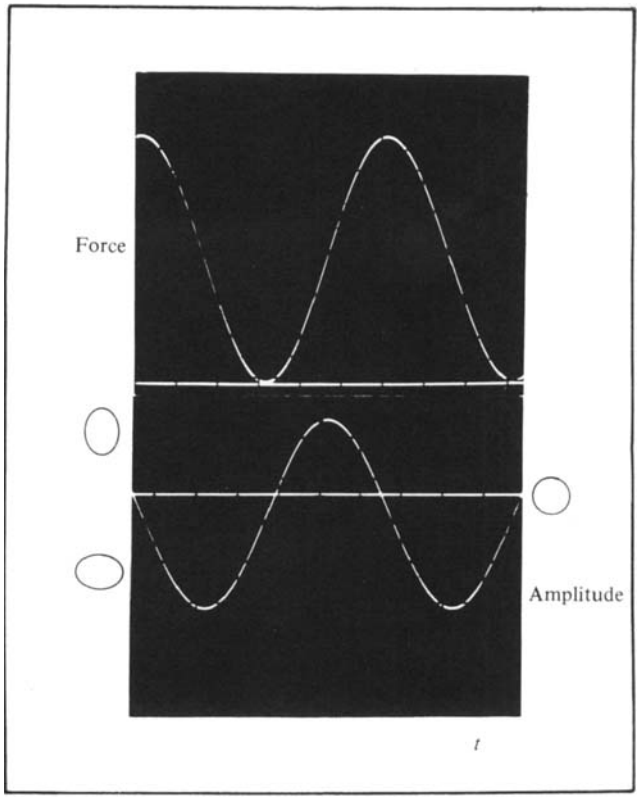

FIGURE 2. Time variations of the acoustic driving force and of the drop response. The drop oscillations are shown to be sinusoidal and lagging in phase by approximately 90°. A bias in favour of the oblate configuration is shown in this particular case.

Taking the time average of this force over f_{m}^{-1}:

$$\langle P_{\mathrm{r}} \rangle \sim \langle \tfrac{1}{2}(1+\cos(4\pi f_{\mathrm{m}} t)) \rangle. \tag{3}$$

One sees that the resulting effect yields a steady-state force as well as a slowly varying force. For a small density mismatch between the drop and the host liquids, this steady force is sufficient to trap the drop at a stable position, and may also introduce a small static deformation of the drop. The equilibrium shape about which the drop oscillates is no longer spherical, but depends upon the magnitude of the force component.

For the axisymmetric case, and in the linear approximation, the deviation of the drop shape from sphericity $x(\theta,t)$ $(= r(\theta,t) - R_0$, where $r(\theta,t)$ describes the drop boundary and R_0 is the radius of the sphere of equal volume) can be expressed as

$$x(\theta,t) = \sum_{n=2}^{\infty} [x_n^{\mathrm{stat}} + x_n \cos(4\pi f_{\mathrm{m}} t + \phi_n)] P_n(\cos\theta), \tag{4}$$

where $P_n(\cos\theta)$ is a Legendre polynomial.

The summation is over all possible shapes of the drop ($n = 2$ refers to the fundamental (quadrupole) mode). x_n^{stat} denotes the static distortion resulting from the

steady component of the radiation-pressure force. Under the present experimental conditions the following relationships are assumed to hold:

$$x_2 \gg x_n^{\text{stat}}, \quad x_2 \gg x_{n+2}. \tag{5}$$

In the case of a 22 kHz standing wave, the periodically oscillating component drives the drop into the oblate shape, while the interfacial tension provides the restoring action. Figure 2 depicts the time dependence of the driving force $F_R(t)$ and the ideal response of the drop at resonance. The response is assumed to be sinusoidal, and lagging in phase by 90°. One should note that the acoustic radiation force never becomes negative.

3.3.2. *Two standing waves.* The experimental conditions pertaining to this work also involve a 22 kHz standing wave used to position the drop, and a time-modulated 66 kHz wave used for the oscillation drive. In this case the voltage across the transducer becomes

$$V_T = V_p \sin(2\pi f_p t) + V_c \sin(2\pi f_c t) \sin(2\pi f_m t), \tag{6}$$

and (4) becomes

$$x(\theta, t) = \sum_{n=2}^{\infty} [x_{pn}^{\text{stat}} + x_n^{\text{stat}} + x_n \cos(4\pi f_m t + \phi_n)] P_n(\cos\theta), \tag{7}$$

where x_p^{stat} is the drop static distortion introduced by the additional positioning field. In the present case we also have

$$x_2 \gg x_{pn}^{\text{stat}}. \tag{8}$$

Assuming that we have a situation where the drop is periodically elongated at the poles, an additional complication arises. Upon inspection (see figure 1) one realizes that the levitating field will exert a force on the liquid in the elongated parts of the drop. The extent to which the acoustic field interferes with the free motion of the drop will depend on the strength of the levitating standing wave. For a nearly neutrally buoyant drop (i.e. $\delta\rho/\rho \leqslant 0{\cdot}005$), such an effect will remain quite small, and could be neglected if one further restricted the oscillations to small amplitudes. On the other hand, in the case of large-amplitude oscillations this additional factor must be accounted for.

4. Resonance-frequency dependence on oscillation amplitude

4.1. *Free decay*

4.1.1. *Experimental results.* A measure of the free decay frequency of an oscillating drop may be obtained from either oscilloscope records, or motion-picture analysis. The procedure consists of first driving the drop into steady-state oscillations in the vicinity of the resonance frequency, abruptly shutting off the excitation, and observing the decay phase. The amplitude dependence may be studied by measuring the decay frequency while gradually increasing the steady-state drive, or by measurements at a different time after the drive termination.

The time variations of the drop shape are obtained through an optical technique monitoring the dimensions of the drop along its vertical (or horizontal) major axis. The shadow of a drop placed in the path of a collimated light beam (5 cm in diameter) is focused, and centred on a narrow slit. The image of this slit is in turn focused on a phototransistor which follows the variations in light intensity due to the drop

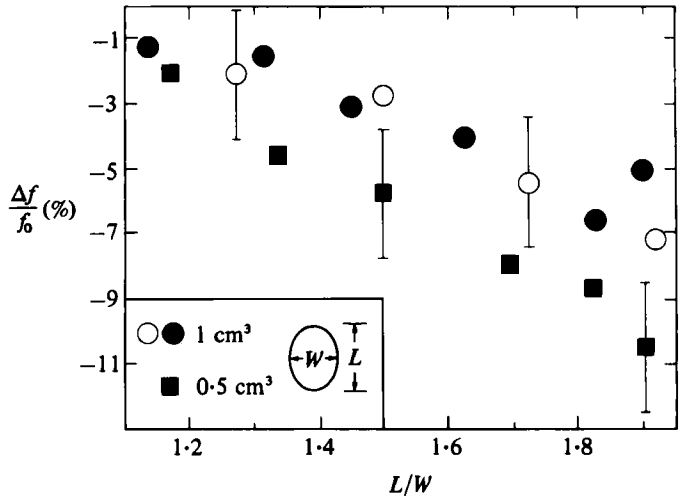

FIGURE 3. Relative change in the free-decay frequency as a function of the initial oscillation amplitude. The axial ratio L/W is measured at maximum deformation during the steady-state drive prior to the free decay phase. The drop are of a silicone oil/CCl_4 mixture, and are immersed in distilled water.

deformations. The variations of the r.m.s. voltage from the photodetector has been measured as a function of the oscillation amplitude, and a linear behaviour has been obtained up to a maximum axial ratio of 1·85 for a prolate ellipsoidal shape.

The free decay frequency can be determined with a relative uncertainty of $\pm 1\,\%$.

A sample of the experimental results is shown in figure 3 for two characteristic drop sizes: 0·5 cm³ and 1·0 cm³ (the drop radii are equal to 0·49 cm and 0·62 cm respectively). The results are for drops of a silicone oil/CCl_4 mixture immersed in distilled water and for a prolate-biased initial oscillation drive. The percentage of the relative change in the decay frequency is plotted as a function of the maximum deformation with the drop in the prolate shape. This latter characteristic is quantified by the ratio of the major over the minor axis. f_0 is the measured free decay frequency for very-small-amplitude oscillations. The initial shape oscillations were provided by a modulated 66 kHz standing wave, and the equilibrium shape was slightly prolate.

Under these conditions, the linear theory would provide the following description of the drop deformation after the oscillation drive is turned off at $t = 0$:

$$x(\theta, t \geqslant 0) = \sum_{n=2}^{\infty} [x_{pn}^{stat} + x_n' \cos(2\pi f_n' t + \phi_n') \exp(-b_n' t) + x_n'' \cos(2\pi f_n'' t + \phi_n'') \exp(-b_n'' t)] P_n(\cos\theta). \tag{9}$$

The single-prime term describes the decay of the steady deformation induced by the oscillation drive, and the double-prime term the decay of the driven shape oscillations. At $t = 0$, and comparing with (7), one has

$$x_n' = x_n^{stat}, \quad \phi_n' = 0, \quad x_n'' \cos\phi_n'' = x_n \cos\phi_n. \tag{10}$$

In this particular experiment we have the conditions

$$x_2'' \gg x_{n+2}'', \quad x_2'' \gg z_{pn}^{stat}, \quad x_2'' \gg x_2' \gg x_{n+2}'. \tag{11}$$

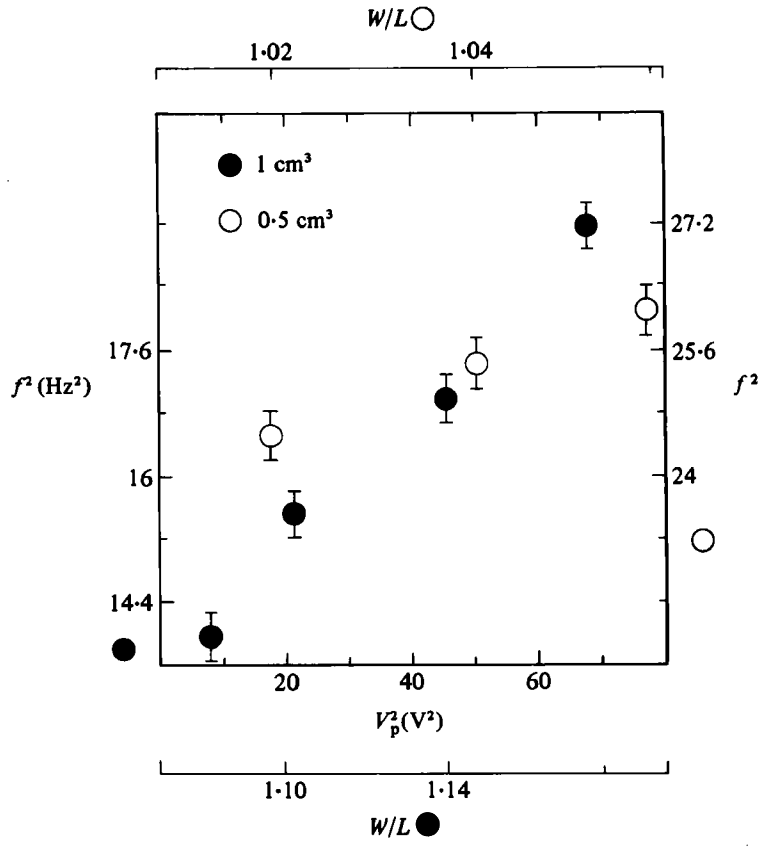

FIGURE 4. Variations of the free-decay frequency as a function of the positioning voltage (V_p^2), and of the static distortion W/L for 0·5 and 1 cm³ drops.

According to available linear theories (Prosperetti 1980*a*, *b*), f_n', f_n'', b_n', and b_n'' are time-dependent, and should approach constant values only in the asymptotic regime. The experimental determination of the free decay frequency for *small-amplitude* initial oscillations has revealed, however, that this parameter was constant. We have therefore assumed that for the low viscosity of the two liquids considered here, and the relatively large size of the drops, this asymptotic regime is attained on a timescale small compared with the fundamental period of oscillation.

Similar results were obtained for the free-decay frequency when the initial forced oscillations were provided by an oblate-biased mechanism.

Information regarding the effects of the steady acoustic positioning force may be obtained from an investigation of the dependence of the resonance frequency upon its magnitude for both small- and large-amplitude oscillation. Figure 4 is a plot of the resonance frequency squared as a function of the positioning voltage squared (V_p^2), for drops having volumes equal to 0·5 and 1·0 cm³, and for *small-amplitude oscillations* ($x_2'' \ll R_0$). An approximately linear dependence may be obtained within the experimental uncertainty. An extrapolation to zero voltage should yield the approximate resonance frequency in the absence of the acoustic positioning force. The data given by figure 3 has been obtained with V_p^2 always less than 9 V².

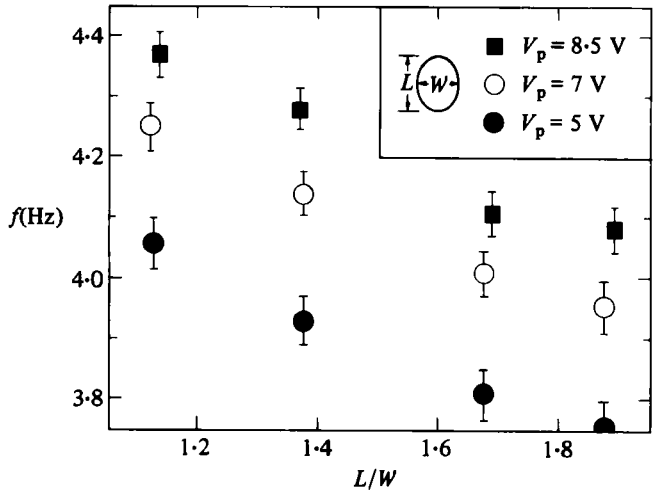

FIGURE 5. Measured free-decay frequency as a function of both the initial oscillation amplitude and the levitation (positioning) voltage.

Decay from steady prolate drive			
Maximum prolate deformation L/W...	1·65	1·75	1·82
$\frac{T_{\text{prolate}}}{T_{\text{cycle}}}$	0·53	0·55	0·56
$\frac{T_{\text{oblate}}}{T_{\text{cycle}}}$	0·47	0·45	0·44
Decay from initial static prolate deformation			
Initial prolate deformation L/W...	1·40	1·57	
$\frac{T_{\text{prolate}}}{T_{\text{cycle}}}$	0·60	0·61	
$\frac{T_{\text{oblate}}}{T_{\text{cycle}}}$	0·40	0·39	

TABLE 1. Variations of the distribution of the two configurations characteristic of the fundamental mode as the oscillations amplitude is increased. The results are for free decay from steady-state oscillation driven by the prolate-biased mechanism, and for free decay from a static deformed prolate shape.

Figure 5 displays the results of free-decay frequency measurements when both the oscillation amplitude and positioning force intensity are varied for a 1 cm^3 drop. One finds that the upward shift in resonance frequency (due to the larger levitation force) remains relatively constant as the amplitude of the oscillations is increased.

An analysis of the asymmetry in the distribution of the oblate and prolate phases during free decay has revealed some interesting results. Two procedures have been used: the first one involves the study of the decay phase of the oscillatory motion after the termination of a steady-state drive, and the second method consists of statically deforming the drop into the prolate or oblate shapes and observing the decay phase subsequent to the nulling of the deforming force. The data are given in table 1, where the percentage of the period spent in each phase is listed as a function of the maximum

Maximum oblate distortion

Cycle number after termination of the steady drive	$W/L = 1{\cdot}75$		$W/L = 1{\cdot}31$	
	$\frac{T_{\text{oblate}}}{T_{\text{cycle}}}$	$\frac{T_{\text{prolate}}}{T_{\text{cycle}}}$	$\frac{T_{\text{oblate}}}{T_{\text{cycle}}}$	$\frac{T_{\text{prolate}}}{T_{\text{cycle}}}$
1	0·51	0·49	0·51	0·49
2	0·53	0·47	0·53	0·47
3	0·54	0·46	0·55	0·45
4	0·57	0·43	0·60	0·40
5	0·60	0·40	0·64	0·36

Decay from static oblate distortion

Initial static oblate distortion

Cycle number	$W/L = 1{\cdot}4$		$W/L = 1{\cdot}21$	
	$\frac{T_{\text{oblate}}}{T_{\text{cycle}}}$	$\frac{T_{\text{prolate}}}{T_{\text{cycle}}}$	$\frac{T_{\text{oblate}}}{T_{\text{cycle}}}$	$\frac{T_{\text{prolate}}}{T_{\text{cycle}}}$
1	0·52	0·48	0·54	0·46
2	0·54	0·46	0·56	0·44
3	0·58	0·42	0·63	0·37
4	0·60	0·40		
5	0·64	0·36		

TABLE 2. Time variations of the configuration distribution during decay from steady-state oscillations driven by the oblate-biased mechanism, and from an oblate static shape. These results show an enhancement of the duration of the prolate configuration with larger amplitude.

prolate (or oblate) deformation during steady-state oscillation, or during the static deformation state. The measurements have been taken during the first full period immediately after termination of steady drive, or after the release of the steady distortion. The data were obtained from high-speed motion pictures, and the accuracy in the determination of the duration of each phase was ± 1 frame, resulting in an uncertainty of $\pm 3\%$ in the time distribution of each configuration.

In the case of oscillations initially driven by the prolate-biased mechanism, the dominance of this configuration is increased as the oscillation amplitude grows larger. This asymmetry is almost totally removed, however, when the oscillations are damped to small values. One might attribute this dominance of the prolate shape to the non-spherical equilibrium shape induced by the steady-state component of the radiation-pressure force. Additional evidence provided by the free decay of oscillations initially driven by the oblate-biased mechanism suggests another explanation. The results of the latter type of experiments show a gradually lengthening duration of the oblate phase as the oscillation amplitude decreases. Because the equilibrium shape in this instance is that of an oblate spheroid, this is a strong indication that large oscillatory excursions enhance the duration of the prolate configuration. Table 2 illustrates the results.

The results of table 1 appear to indicate a slight difference in the time distributions of the shapes. Free decay from a static distortion is seen to accentuate the asymmetry. An additional observation concerning the free decay frequency might also be worth mentioning at this time: it appears that the oscillation frequency measured during the decay phase from a statically distorted shape (prolate or oblate) displays fluctuations not found during the free decay from steady-state driven oscillations.

This could be interpreted as the manifestation of the higher resonant modes from the continuous and discrete spectra (Prosperetti 1980*a*, *b*).

4.1.2. *Discussion.* The results given in figure 5 imply that the static levitation force influences the dynamics of a 0·5 cm^3 drop to a lesser extent than in the case of a 1 cm^3 drop. A phenomenological explanation may be provided by the more significant distortion experienced by the larger drop levitated in the same standing-wave field. The additional surface energy of a distorted shape is reflected in a larger interfacial tension. In addition, even with small static drop deformations, the effect of the positioning acoustic field might also contribute to this difference. Finally, the fact that x_2' (equation (9)) is not zero might also influence the above results. A partial explanation of the drop size dependence found in the results (figure 3) would therefore be provided by the interference of the acoustic forces, this interference being weaker for smaller-size drops.

It is also possible that the characteristic nonlinearity associated with the large-amplitude oscillations has an inherent drop-radius dependence. A confirmation of such a hypothesis can only be provided by a nonlinear theory. Such an undertaking is beyond the scope of this work.

In any case, there are strong indications that the natural frequency (measured during free decay) decreases with increasing amplitude for shape oscillations in the fundamental mode. A relative decrease of 10·5 % has been measured for a 0·5 cm^3 drop undergoing oscillations characterized by a maximum deformed prolate shape with an axial ratio of 1·9. The true value of the frequency shift may be slightly higher, and would be measured in the absence of any additional static force.

4.2. *Driven oscillations*

4.2.1. *Swept frequency response.* An alternative method for the measurement of the resonance frequency is provided by the swept-frequency response of the drop. In principle, this technique allows the determination of the resonance curve, and the measurement of the damping constant through the experimental Q-value. In this work, the modulation frequency is varied linearly within a range bracketing the drop fundamental mode. The sweep rate used is 10 mHz/s, and the sweep time is 100 s.

The two available driving modes have also been used with apparently contradictory results: the fundamental resonance frequency was shown to decrease with increasing oscillation amplitude when the drive providing an elongation of the drop was chosen, but the reverse was obtained with the opposite driving mode.

The results are shown in figures 6 and 7. Figure 6 reproduces the experimental resonance curves obtained at various oscillation amplitudes, and with the 'elongating' drive supplied by a modulated 66 kHz standing wave. Figure 7 gives similar results for the opposite driving mode. The ordinate scales on figures 6 and 7 are not the same; the displacements represented by the curves of figure 6 are significantly smaller than those shown in figure 7.

Figure 8 is a plot of the measured shift in resonance frequency as a function of the ratio L/W for both driving modes. The frequency increase associated with the oblate-biased mode is found to be significantly less than the frequency decrease resulting from the opposite driving mode.

4.2.2. *Steady-state oscillations.* Figure 9 illustrates the increasingly larger bias towards the prolate configuration when a 1 cm^3 drop is excited by the appropriate

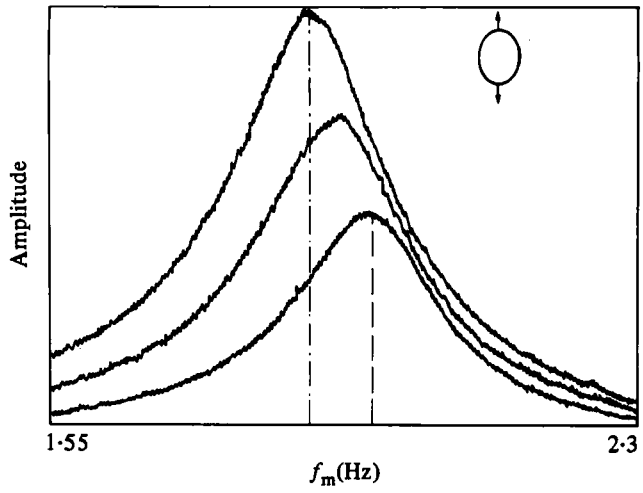

FIGURE 6. Swept frequency response of a 1 cm³ drop around its fundamental ($L = 2$) resonance mode. The oscillation drive is prolate-biased, and the various curves have been obtained for increasingly larger excitations. The oscillation amplitudes are large ($x_2/R_0 \geqslant 0{\cdot}1$).

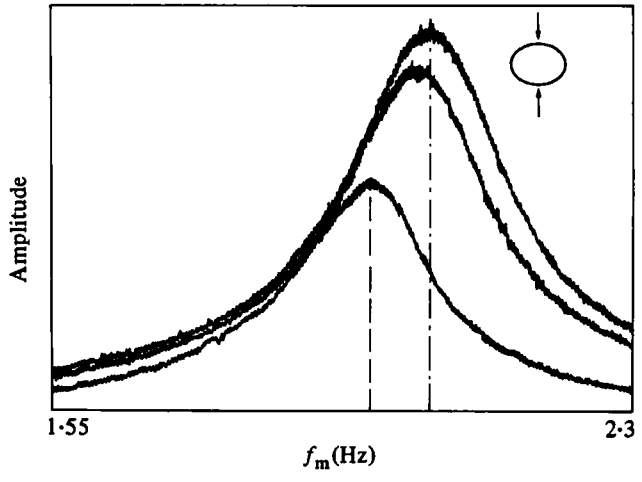

FIGURE 7. Swept frequency response of the same drop as in figure 6, except that the oblate-biased drive has been used. ($x_2/R_0 \geqslant 0{\cdot}2$).

drive. One finds that the prolate configuration occupies a considerably longer time as the oscillation amplitude grows larger. These photographs have been obtained under strobed illumination whose phase relationship with respect to the driving force could be varied at will. Shown here are the mid-plane profiles with the symmetry axis vertical in the plane of the picture. The phases associated with the various configurations are measured with respect to the spherical shape (arbitrarily used as a reference 360°).

A symmetrical reversal of the time distribution of the two configurations does not take place, however, when the opposite driving mode is used. Observations of the steady-state, large-amplitude, oblate-biased forced oscillations have revealed that the fraction of the oscillation period during which the drop is in the oblate shape cannot

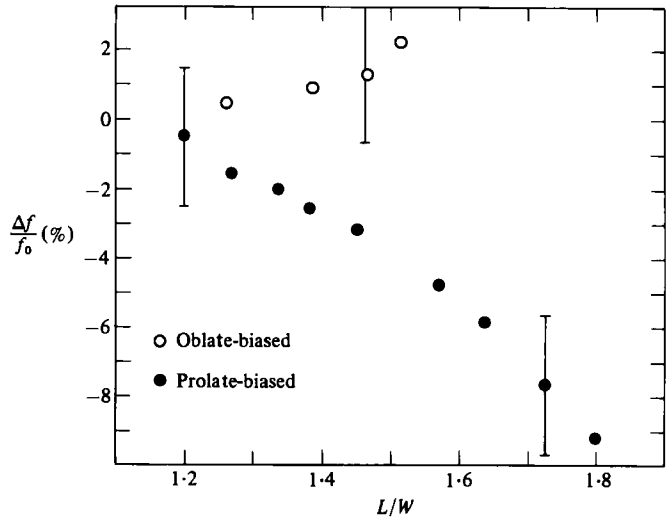

FIGURE 8. Measured peak-frequency shift as a function of the oscillation amplitude for both driving modes.

be made to dominate as significantly as in the case of the prolate-biased drive. Even for significant oscillation amplitudes ($x_2/R_0 \geqslant 0{\cdot}3$), the time distribution of the two configurations remains roughly balanced, i.e. $T_{\text{oblate}} \approx T_{\text{prolate}}$.

5. The damping of large-amplitude oscillations

The damping rate of oscillating drops has been measured as a function of the oscillation amplitude through high-speed motion-picture analysis, as well as through oscilloscope decay traces. Some representative results are reproduced in figure 10.

The data-gathering procedure is as follows. The drops are first driven into steady-state oscillations at the fundamental resonance frequency; the acoustic excitation is then cut off, and the decay process is recorded on the oscilloscope and high-speed ciné films. The initial conditions are

$$x_2'' \gg x_{n+2}'', \quad x_2'' \gg x_{pn}^{\text{stat}}, \quad x_2'' \gg x_2' \gg x_n', \quad x_2''/R_0 \geqslant 0{\cdot}1.$$

Figure 10 reproduces the decay curves for individual drops on a semi-logarithmic scale. A striking exponential behaviour is obtained for the various initial excitations, although the measured decay rates appear to be different for different initial L/W. This appears to suggest that in this case the rate of energy dissipation is controlled by the initial conditions. This is quite plausible because the established flow-field configurations both inside and outside the drop will no doubt influence the damping of the motion. Thus, the decay mechanism of large-amplitude drop-shape oscillations is characterized by a fixed constant rate which appears to depend on the initial established flow fields.

The rate of decay has been measured from the first oscillatory cycle after the termination of the steady-state drive. This decay rate is not only that denoted by b_2'' (see (9)), but also includes a contribution from b_2, since $x_2' \neq 0$.

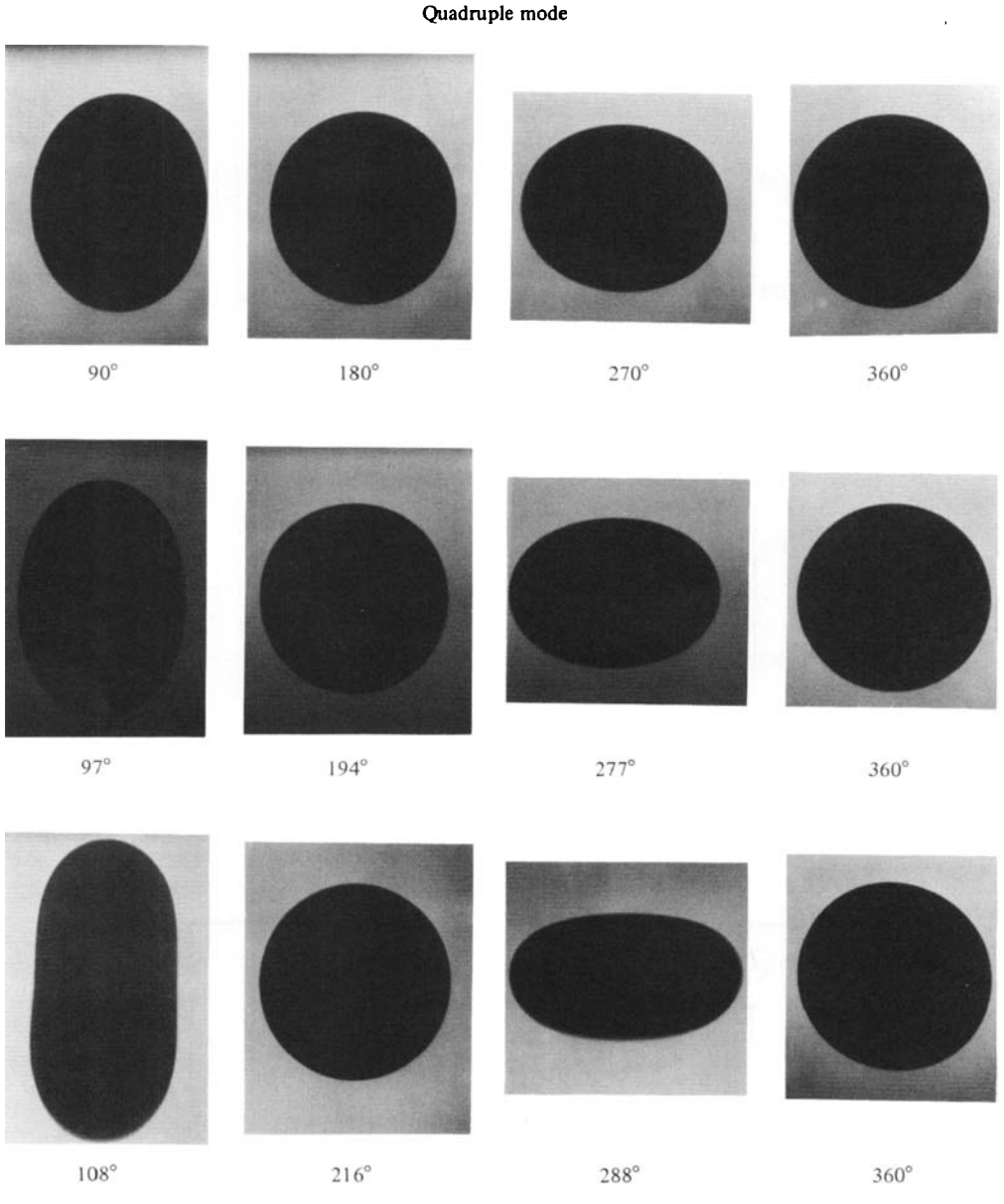

FIGURE 9. Time distribution of the prolate and oblate configurations during steady-state drive supplied by the prolate-biased mechanism. A nearly spherical shape is arbitrarily chosen as the reference configuration (360°).

Figure 11 shows the measured damping rate for different drops. For each individual drop the decay rate is measured for increasingly larger initial oscillation amplitudes. This latter parameter is represented by the ratio L/W plotted along the abscissa and measured in the steady-state phase. The relative large experimental uncertainty ($\pm 5\%$) does not allow any definitive conclusion, although one could perceive a slight increasing trend with larger axial ratios.

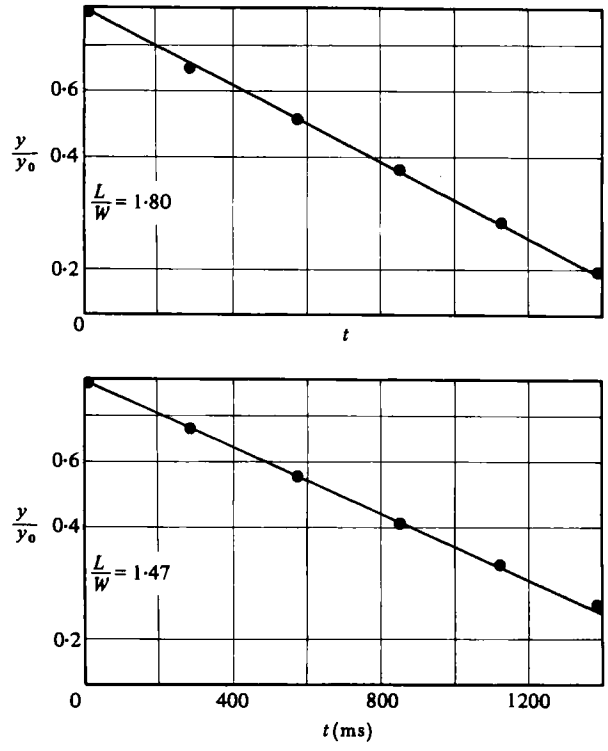

FIGURE 10. Semi-logarithmic plot of the time evolution of the oscillation amplitude during free decay for a 1 cm³ drop.

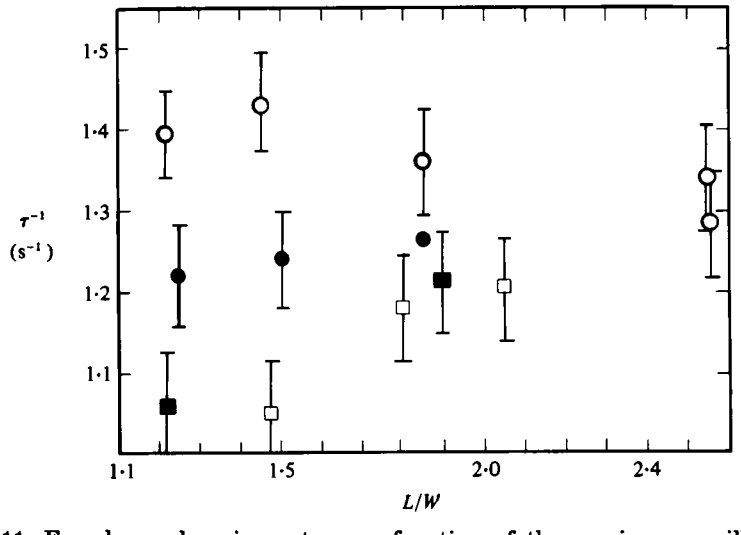

FIGURE 11. Free-decay damping rate as a function of the maximum oscillation amplitude. ■, □, 1 cm³ drops; ●, 0·7 cm³ drops; ○, 0·5 cm³ drops.

The present experimental study has not revealed any inherent time dependence for the damping parameter even for small-amplitude oscillations. Such a dependence has been suggested on the basis of theoretical analysis (Prosperetti 1980*a*, *b*), but such a phenomenon does not appear to be a characteristic of the decay of an initially oscillating drop in the resonant mode.

6. Internal flow fields

A study of the characteristics of the internal flow fields within oscillating drops is a natural approach to the problem raised by the observed phenomena cited in the preceding sections. Such an experimental study has not yet been attempted for the case of liquid drops undergoing large-amplitude shape oscillations. A photographic technique using the streak patterns of suspended dye particles has been used in this work to yield two-dimensional pictures of the fluid-particle flow fields.

Organic dye particles with size ranging between 5 and 50 μm are dispersed in the drop liquid. The particles close to the central midplane containing the symmetry axis are illuminated by a plane light sheet, and the 90° scattered light is photographed while the drop is driven into steady-state oscillations. The exposure usually lasts for a few oscillatory cycles. Figures 12 and 13 reproduce the resulting streak patterns of oscillating particles situated in the plane containing the symmetry axis. These photographs show the evolution of the fluid flow pattern as the oscillation amplitude is increased. All drops are undergoing steady-state oscillations in the fundamental mode.

In figure 12 the maximum oscillation amplitude resulting in the bottom-right pattern is on the order of 20 % of the equilibrium spherical radius. The pattern of the upper-left picture results from a relative amplitude amounting to about 5 %. The essential feature of these internal flow fields is the gradual spreading towards the centre of a steady circulation superposed upon the oscillatory motion. This phenomenon is better illustrated in figure 13, where the oscillation amplitude is varied from 8 % to 20 % of the equilibrium radius. In photograph (*a*) the steady drifting motion of the fluid particles appears limited to the outermost parts of the drop. Photographs (*b*) and (*c*) reveal a spreading of this steady motion to the inner drop regions. Note, however, that even in photograph (*c*) the centre of the drop remains motionless, and the particles along the two intersecting axes still undergo a strictly linear oscillatory motion. Together with the spreading of the circulatory motion, the velocity of this steady drift also increases as the amplitude grows. Photograph (*d*) is a seemingly erratic oscillatory motion. No distinct pattern can now be distinguished, although the basic fourfold symmetry is still preserved.

Similar phenomena may be observed within a drop oscillating in the $L = 3$ mode. In addition to the characteristic modification in the flow pattern associated with the oscillatory mode, a difference arises in the threshold for the appearance of circulation: the onset of the steady drifting motion is characterized by a substantially smaller oscillation amplitude than in the $L = 2$ mode. Figure 14 reproduces photographs of the two different drops undergoing vibrations in the $L = 3$ mode. The upper row of photographs reveals a substantially more disordered pattern as the vibration amplitude is increased. The lower row shows a well-defined circulation together with the disappearance of the characteristic symmetry. An additional property of interest is

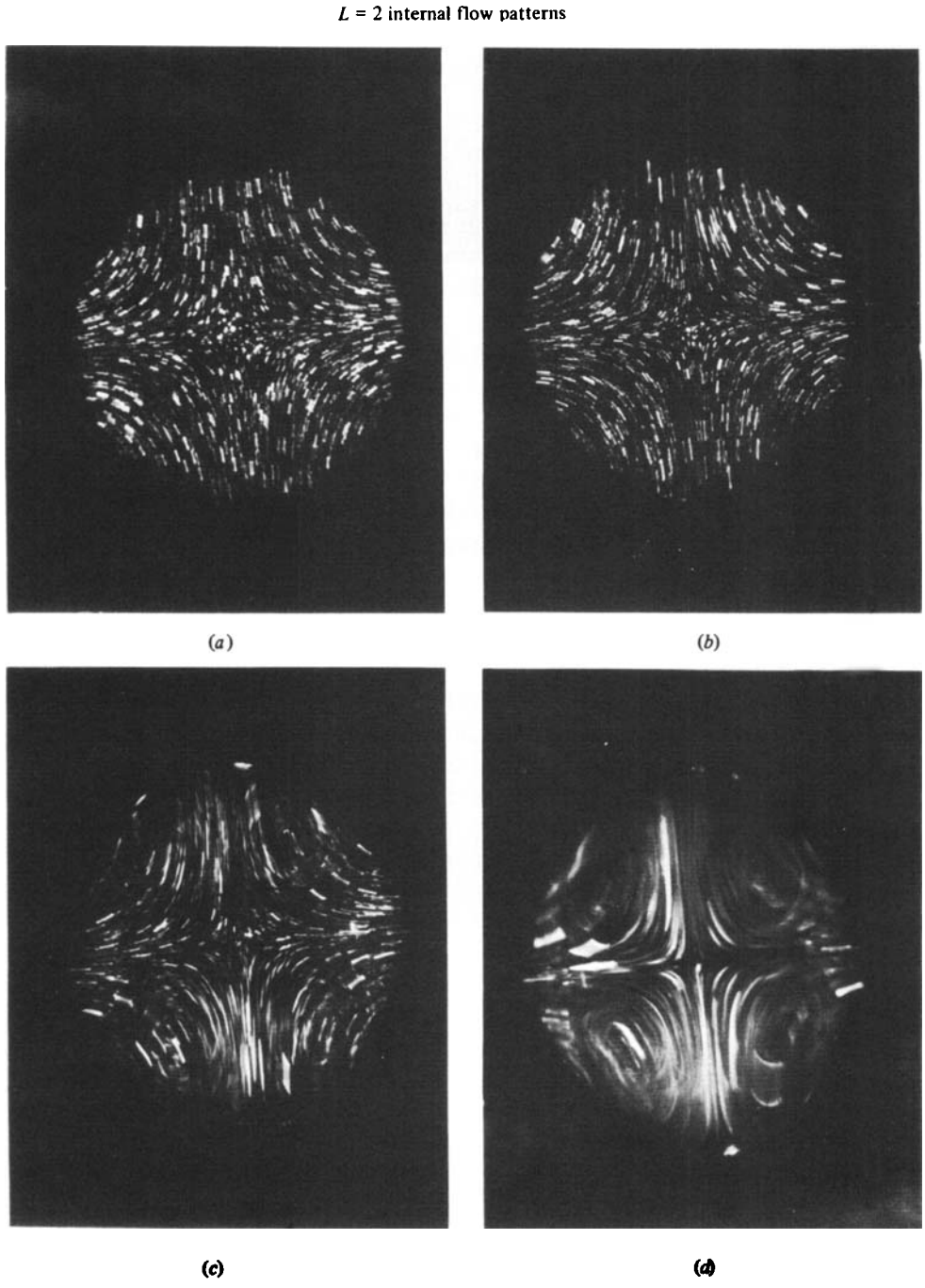

FIGURE 12. Streak patterns of suspended dye particles in the midplane of an oscillating drop in the $L = 2$ mode. The drop liquid is silicone oil (50 cSt), and the host liquid is a mixture of distilled water and methanol. The appearance of a steady drifting motion is visible as the oscillation amplitude is increased. The Reynolds number varies from about 2 to 10.

L = 2 internal flow patterns

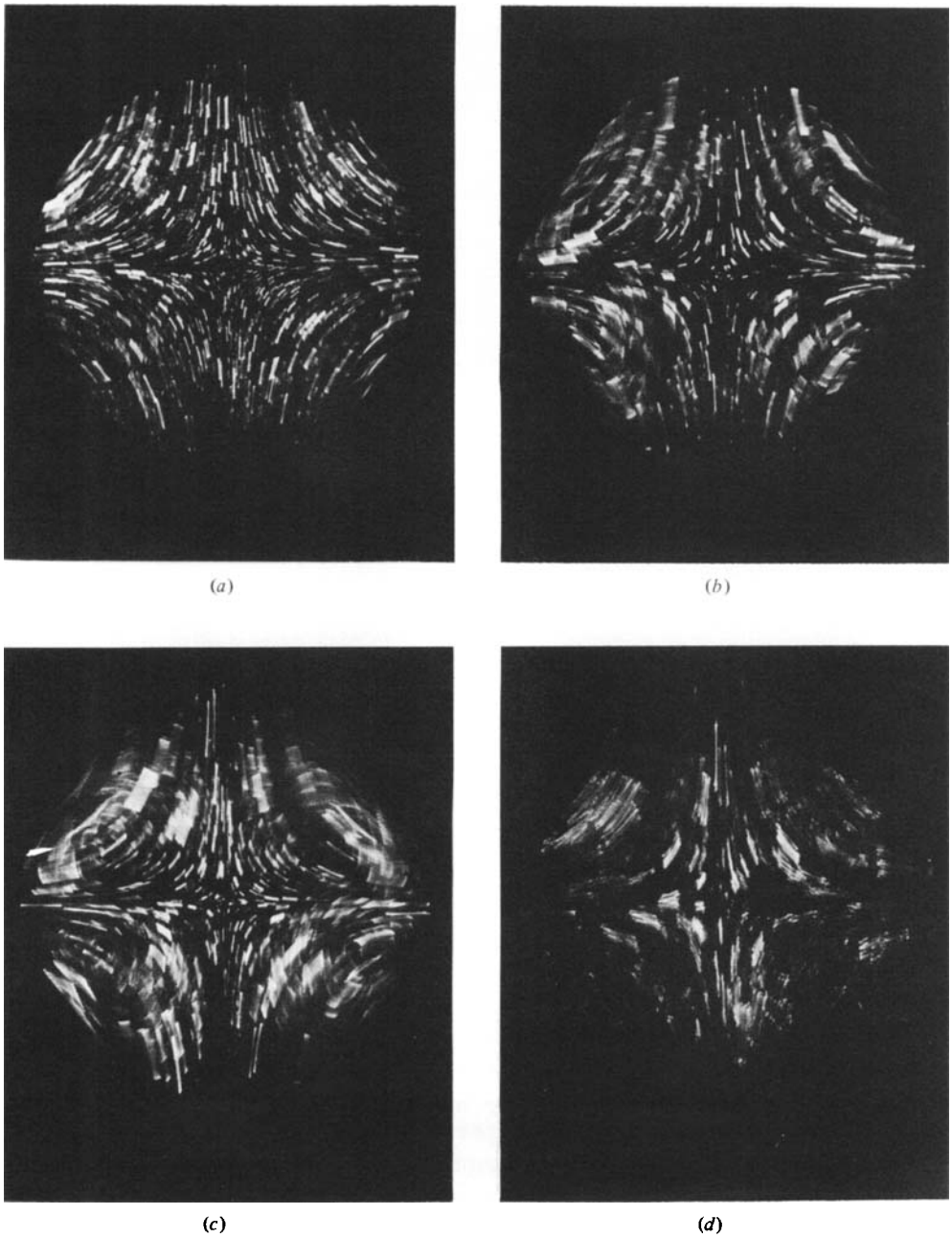

(*a*) (*b*)

(*c*) (*d*)

FIGURE 13. Same as figure 12. The 1 cm^3 drop is made of a silicone-oil–CCl_4 mixture (3·2 cSt), and is immersed in distilled water.

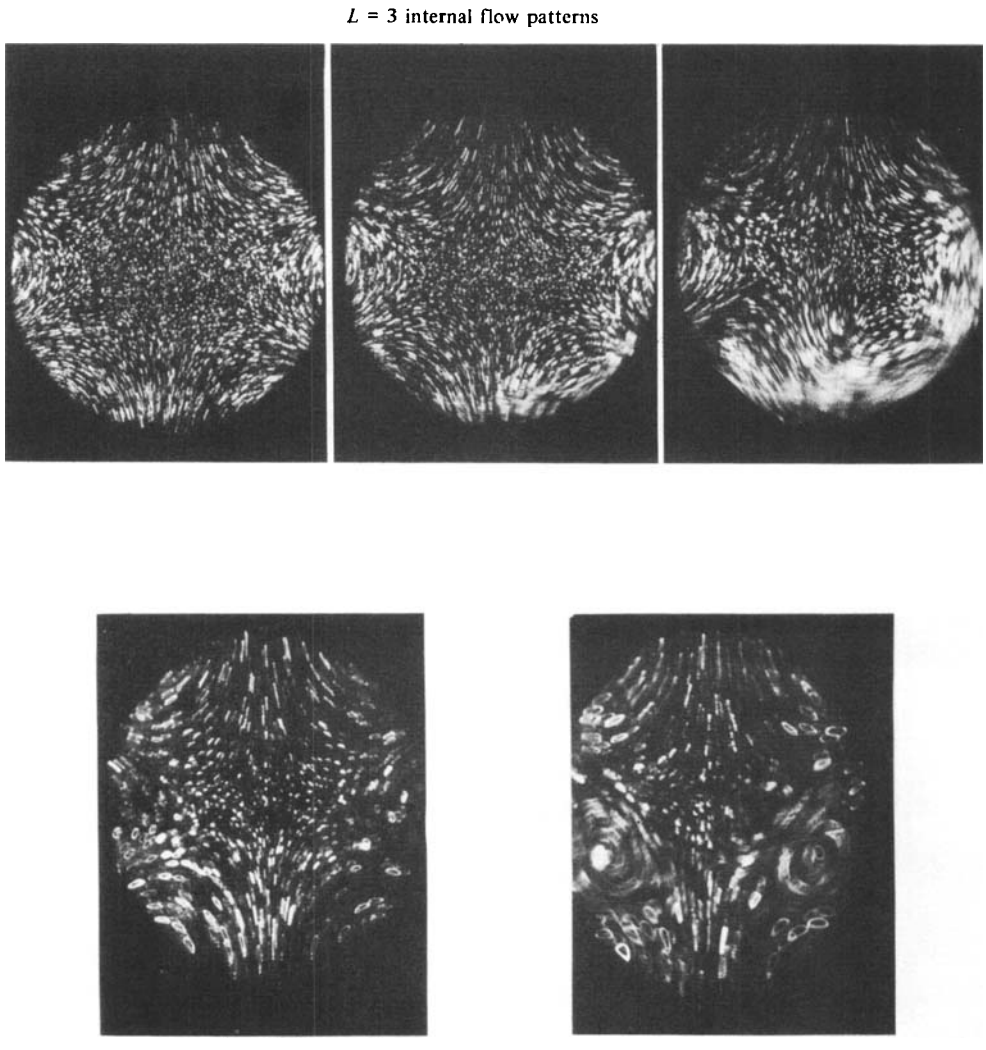

FIGURE 14. Streak pattern within a 1·5 cm³ drop (3·2 cSt silicone-oil–CCl_4 in water in the upper row, 50 cSt in water–methanol in the lower row) oscillating in the $L = 3$ mode.

the closed path taken by some oscillating particles no longer moving along a linear trajectory. The consistent appearance of the circulatory pattern in the bottom half of the drop is probably an artifact caused by the asymmetry in the acoustic field.

No systematic treatment of the flow pattern in the outside host liquid has been undertaken in this work because the emphasis has been placed upon phenomena involving the drop itself. There is no obvious reason, however, why the same technique could not be used for a similar qualitative study of the external flow field.

7. Rotational motion

An additional phenomenon arises when the oscillation amplitude attains a substantial value: the onset of an apparent rotational instability. Such a rotation can easily be observed during large-amplitude steady-state oscillations, and it reveals

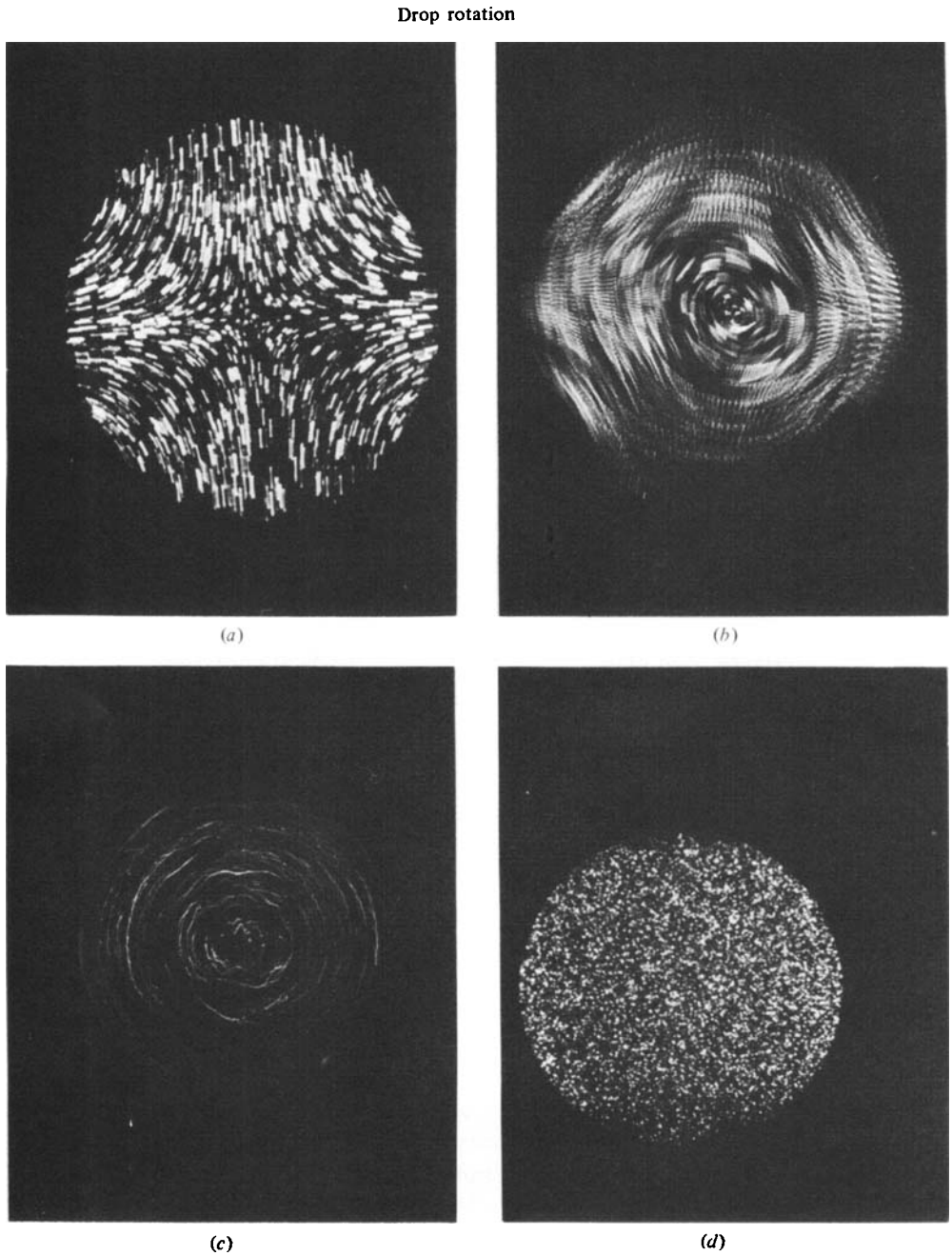

FIGURE 15. Dye-particle flow patterns for oscillating, rotating-and-oscillating, rotating, and still drops.

itself at first as a running wave on the drop surface which subsequently develops into a solid-body rotation of the drop fluid.

Figure 15 reproduces photographs of an oscillating drop in the $L = 2$ mode (*a*), a rotating–oscillating drop (*b*), a rotating drop after the oscillation drive has been terminated (*c*), and finally a quiescent drop at equilibrium (*d*).

The origin of such an 'instability' is not yet clear. It might be associated with the characteristics of large-amplitude oscillations, but it could also arise because of the asymmetry and misalignment of the drop in the acoustic field.

The appearance of the drop rotation does not depend only on the oscillation amplitude, but also shows a very marked dependence upon its frequency. It appears that the onset of surface particle rotation can always be started when the drive frequency is slightly higher than the drop resonance frequency, but such rotation never takes place if the drive frequency is maintained at or below the drop resonance frequency. This latter frequency continuously shifts to lower values as the oscillation amplitude increases.

Because of this frequency dependence one might conjecture that there exists an independent running wave mode with a slightly higher resonance frequency than the $L = 2$ mode. Another possibility, however, may also be that a misalignment of the drop axis with respect to that of the acoustic field leads to a net torque on the drop. An analysis reveals that such a destabilizing torque arises only when the drop response lags the oscillation drive in phase by an angle larger than 90°, a situation which would arise with a drive frequency higher than the drop resonance frequency. It is unfortunately not yet possible to make a definitive statement as to which is the correct answer, for the perfect alignment of the drop axis along the acoustic field is not a trivial experimental matter.

As a last comment, one might add that the rotation is not restricted to the fundamental mode. The onset of the running wave has also been observed for drops oscillating in the $L = 3$ mode.

8. Other phenomena associated with large-amplitude shape oscillations

As the oscillation amplitude is greatly increased, and if the rotational or other instabilities are avoided, the increasingly larger deformation may cause the drop to split. Radiation-pressure-induced drop fission was first observed with 2 mm diameter drops (Marston & Apfel 1980), and our present results confirm that cavitation-free splitting of 1 cm diameter drops is also possible when the acoustic wavelength is comparable to the drop diameter. Figure 16 illustrates the stages of such dynamic fission for a 1 cm^3 silicone oil (50 cSt) drop in water. The formation of the third smaller satellite drop often accompanies the splitting into the two main droplets.

By an appropriate combination of the acoustic forces, it is also possible to excite drops into modes of oscillation which are not the pure resonant shapes, and at frequencies not corresponding to any of the normal modes derived from the linear theory. These odd oscillatory modes are likely to be combinations of the various pure modes, including those involving non-axisymmetric geometries. An example is given by figure 17, where photographs (*a*) and (*c*) are the principal shapes associated with phase lags equal to 90° and 270° respectively, and photos (*b*) and (*d*) are intermediate configurations. This mode is excited at a frequency slightly higher than that corresponding to the $L = 3$ mode for the same drop. The drop liquid is phenetole and the host liquid is a mixture of H_2O and methanol. The oscillation drive is provided by a 66 kHz standing wave.

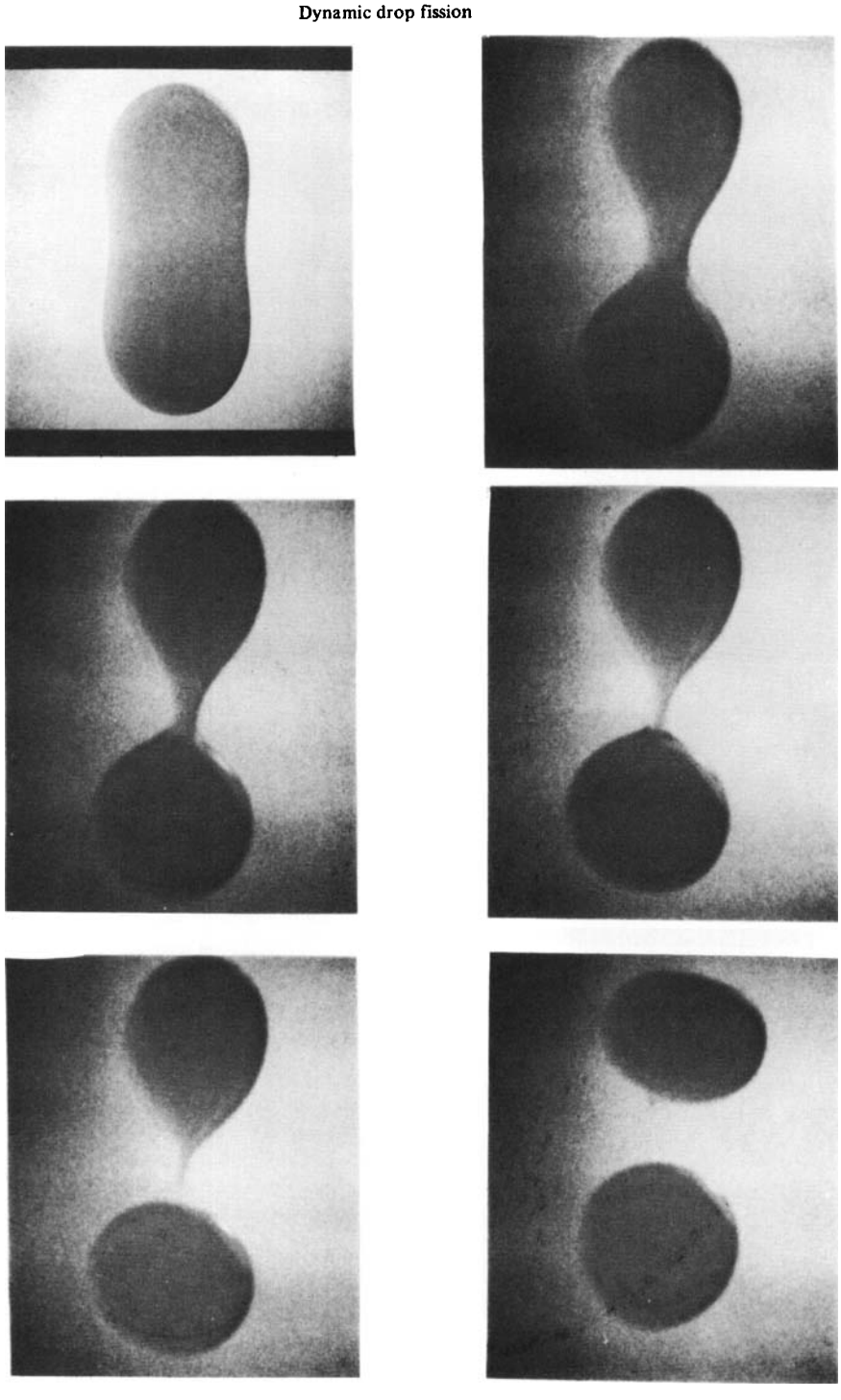

FIGURE 16. Stages of dynamic drop fission by acoustic radiation pressure. The drop is 1·5 cm³ in volume.

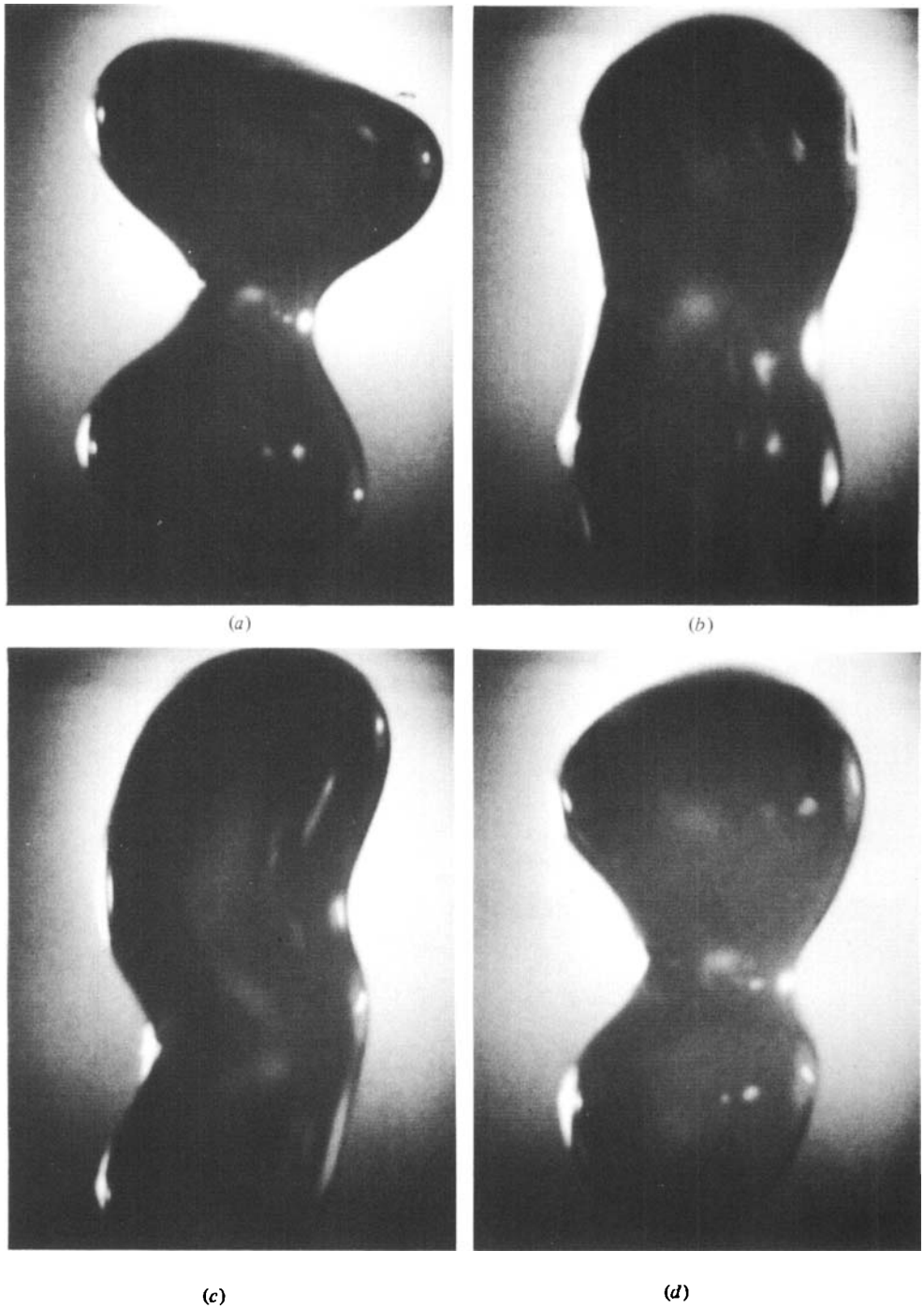

FIGURE 17. Drop oscillating in a non-normal mode.

9. Summary and conclusion

The upward shift in the free decay frequency as the oscillation amplitude is reduced suggests the appearance of a soft nonlinearity in the fundamental resonance frequency. This result is qualitatively similar to the lowering of the resonance frequencies of air bubbles oscillating radially in water ($L = 0$ mode) when the oscillation amplitude is increased (Lauterborn 1976). In the cases of bubbles this behaviour is described by the nonlinear equation of motion whose solutions have been obtained numerically. For the present case of the drop-shape oscillations, however, no successful nonlinear treatment has yet been proposed.

In contrast with the free decay frequency, the decay rate has been shown to be constant for a given initial condition on the oscillation amplitude. As might have been expected, the results of the decay rate measurements reveal a dependence on the established initial conditions. A hint of an increase in the decay rate has been obtained, but no definite quantitative conclusion can yet be drawn.

The qualitative study of the internal flow field of steady-state oscillating drops has revealed flow fields which are more complicated than suggested by the simple linear theory. Circulation has been shown to be present even for the relative oscillation amplitude as low as 8 %, and appears to originate first at the drop boundary and to spread subsequently towards the drop interior.

Finally, the possibility of a rotational instability was investigated, but no confirmation was forthcoming owing to the unresolved dilemma involving the role of the asymmetry of the acoustic field. Dynamic drop fission was demonstrated as well as the existence of modes which cannot be derived from the linear theory.

We wish to thank Prof. Philip Marston for his many helpful suggestions, and Mr E. Olli for his technical advice. This work is supported by the National Aeronautics and Space Administration under contract NAS 7-100.

Appendix

We give in table 3 relevant properties of the liquids used in this study. The values listed are for a temperature of 23 °C.

Liquid	Density (g/cm³)	Sound speed (m/s)	Interfacial tension (dyn/cm)	Kinematic viscosity (cSt)	Figure number
Distilled water	0·998	1503	—	0·95	All except 12, 14, 16
Dow Corning 200 Silicone (5 cSt) + CCl_4	1·001	960	37 (in water)	3·2	3–11, 13, 15, 17 tables 1, 2
Dow Corning 200 Silicone Oil, 50 cSt	0·96	1005	32 (in water + methanol)	50	12, 14, 16
Distilled water + methanol (4:1 by volume)	0·95	1555	—	0·89	12, 14, 16

TABLE 3

REFERENCES

LAUTERBORN, W. 1976 *J. Acoust. Soc. Am.* **59**, 283.
MARSTON, P. 1980 *J. Acoust. Soc. Am.* **67**, 15.
MARSTON, P. & APFEL, R. 1979 *J. Coll. Interface Sci.* **68**, 280.
MARSTON, P. & APFEL, R. 1980 *J. Acoust. Soc. Am.* **67**, 29.
MARSTON, P., LOPORTO ARIONE, S. & PULLEN, G. 1981 *J. Acoust. Soc. Am.* **69**, 1499.
MILLER, C. & SCRIVEN, L. 1968 *J. Fluid Mech.* **32**, 417.
PROSPERETTI, A. 1980*a* *J. Méc.* **19**, 149.
PROSPERETTI, A. 1980*b* *J. Fluid Mech.* **100**, 333.
TRINH, E., ZWERN, A. & WANG, T. 1982 *J. Fluid Mech.* **115**, 453.